Journal of Computational Physics **151,** 212–241 (1999)
Article ID jcph.1998.6176, available online at http://www.idealibrary.com on IDEAL®

A Fast Adaptive Multipole Algorithm for Calculating Screened Coulomb (Yukawa) Interactions

Alexander H. Boschitsch,* Marcia O. Fenley,*,† and Wilma K. Olson†

Continuum Dynamics, Inc., P.O. Box 3073, Princeton, New Jersey 08543; and †Department of Chemistry, Wright and Rieman Laboratories, Rutgers, The State University of New Jersey, 610 Taylor Road, Piscataway, New Jersey 08854-8087

Received June 30, 1998; revised December 1, 1998

The screened Coulomb (Yukawa or Debye–Hückel) potential, $\Phi = \exp(-\kappa r)/r$, where r is the separation distance and κ is the Debye–Hückel screening parameter, gives a good description of the electrostatic interactions in a variety of biologically and physically important charged systems. It is well known that the direct calculation of the energy and forces due to a collection of N charged particles involves the pairwise summation of all charged particle interactions and exhibits an $O(N^2)$ computational complexity which severely restricts maximum problem size. This has prompted the development of fast summation algorithms that allow the electrostatic energy and forces to be obtained in only $O(N \log N)$ operations. To date, however, practically all such implementations have been limited exclusively to pure Coulombic potentials ($\kappa = 0$), and the central contribution of the present method is to extend this capability to the entire range of the inverse Debye length, $\kappa \geq 0$. The basic formulation and computational implementation of the spherical modified Bessel function-based multipole expansions appropriate for the screened Coulomb kernel are first presented. Next, a simple model system consisting of a single source charged particle is studied to show that the maximum electrostatic energy error incurred by an M-order multipole expansion for the Yukawa potential is bounded above by the error of the equivalent multipole expansion for the Coulombic potential. Finally, timing and accuracy studies are presented for a variety of charged systems including polyelectrolyte chains, random distributions of charges inside a cube, and face-centered-cubic lattice charge configurations containing up to 103,823 charges.

Key Words: electrostatics; Yukawa potential; Debye–Hückel potential; screened Coulombic interactions; fast multipole method; polyelectrolyte.

0021-9991/99 $30.00

1. INTRODUCTION

Electrostatic interactions play a major role in many molecular systems, and considerable effort is being devoted to the accurate and efficient computer modeling of large-scale physically realistic charged systems. Because of their long-range nature, all interactions between charged particles must be accounted for so that the exact calculation of the electrostatic energy and forces by direct summation requires $O(N^2)$ operations. To alleviate this high computational burden, much research has been directed toward the development of so-called fast summation methods which combine hierarchical grouping procedures and multipole expansion approximations to realize $O(N \log N)$ operation counts [23, 26, 27]. To date, such methods have been limited to systems governed by pure Coulombic potentials. Many molecular systems of biological and physical significance, however, are governed by the screened Coulomb (also called the Debye–Hückel or Yukawa) potential. Fast summation methods are not currently available for charged systems governed by the Yukawa potential, and the focus of the present paper is to formulate and implement a new fast adaptive multipole algorithm suitable for such systems.

The total screened Coulomb electrostatic energy of a system containing N charged particles, is given by

$$U_e = \frac{1}{\varepsilon} \sum_{i=1}^{N} \sum_{j=1}^{i-1} \frac{q_i q_j}{r_{ij}} e^{-\kappa r_{ij}}, \tag{1}$$

where κ is the Debye–Hückel screening parameter (which is proportional to the square root of the ionic strength of the solution), q_i is the charge of particle i, ε is the dielectric constant of the solvent, and r_{ij} is the separation distance between particles i and j. Equation (1) characterizes problems where electrostatic interactions are attenuated by a background ionic medium. When $\kappa = 0$, this expression reverts to the form for pure Coulombic interactions. It should be noted that Eq. (1) describes the solvent solely by its dielectric constant (i.e., dielectric continuum approximation) and the screening effect of the ionic species in solution by the exponential term ($e^{-\kappa r}$). Hereafter the direct summation of all $N(N-1)/2$ pairwise electrostatic interactions in Eq. (1) will be termed the "direct summation method."

The screened Coulombic potential, $\exp(-\kappa r)/r$, has been extensively used to model intermolecular/intramolecular electrostatic interactions in a wide range of physical and macromolecular systems such as charge-stabilized colloids [48, 57], weakly charged polyelectrolytes [11, 29, 62], lattice polyelectrolytes [2], dendritic polyelectrolytes [65], biopolyelectrolyte DNA [21, 51], ionic micellar solutions [67], and colloidal (dusty) plasmas [28, 59]. The study of Yukawa systems usually involves Monte Carlo (MC) or molecular dynamics (MD) simulations [2, 19, 33, 63] where the screened Coulombic energy and/or forces are repeatedly evaluated subject to free or periodic boundary conditions. The most computationally demanding aspect of these MC/MD simulations is the direct evaluation of the long-range electrostatic potential energy and/or forces which exhibit $O(N^2)$ computational complexity. Of course, the same is true for MC/MD simulations of charged systems governed by the Coulombic potential.

The boundary element-based solution to the linear Poisson–Boltzmann equation (PBE) is also subject to the $O(N^2)$ behavior due to the mutual screened Coulombic interactions between all N boundary elements [32, 34, 68]. Despite being more accurate than finite-difference-based methods, the boundary element formulation of the linear PBE is not widely used in biomolecular applications due to both CPU and memory demands.

Due to the high costs associated with the direct computation of the electrostatic energy and forces and the importance of large-scale computer simulations of molecular systems, considerable effort has been devoted to developing particle–mesh approaches and tree-based fast multipole methods (FMMs) for solving N-body electrostatic problems, and there now exist numerous, highly efficient $O(N \log N)$ and $O(N)$ implementations for calculating *Coulombic* interactions in both nonperiodic (i.e., isolated systems) and periodic charged systems [6, 8, 12, 15, 18, 22, 23, 27, 37, 38, 53, 66]. For a comparison of the FMM and particle–mesh-based approaches the reader is referred elsewhere [43, 60].

In a particle–mesh-based approach, the collection of charges is essentially replaced by a smoothed charge distribution which may be accurately represented upon a regular mesh. The electrostatic potential due to this smoothed distribution is developed by transforming the problem into frequency space using fast Fourier transforms (FFTs) upon the regular mesh. For M grid points the FFT is accomplished in $O(M \log M)$ operations, which, if $M \log M \ll N^2$, allows CPU reductions to be realized. The potentials induced by a charged particle and its smoothed analogue at a distant point are virtually indistinguishable. For closer (near-field) evaluations, however, the potentials differ markedly and local corrections must be applied to restore global accuracy. Particle–mesh algorithms are attractive because of the straightforward coding requirements and their smooth numerical behavior, which is conducive to deterministic optimization studies. For problems involving volumetric charge distributions that fill the computational domain, particle–mesh algorithms are computationally most effective. Thus, the particle–mesh-based approach for the Ewald sum [12, 14, 18] in molecular dynamics of charged systems that invoke periodic boundary conditions is now widely used in large-scale biomolecular simulations [9, 31, 56, 69].

On the other hand, when studying systems where the charges or active elements are distributed upon surfaces (this is commonly the case in boundary element treatments) or along chains (e.g., polyelectrolyte modeling), performance is likely to degrade. This is because the smoothed problem is still solved upon a full 3D regular mesh, which implies high storage penalties and costs in evaluating the FFTs (i.e., the requirement $M \log M \ll N^2$ becomes more difficult to satisfy). In such problems, FMM techniques are likely to prove more efficient because of the adaptive mesh and hierarchical groupings made possible using octrees.

The fast multipole algorithm developed by Greengard and Rokhlin, which combines the hierarchical grouping of particles with truncated multipole expansion and local Taylor series expansion for the Coulombic potential, was originally developed for 2D charged systems [26, 27]. Spherical harmonics-based fast multipole algorithms were subsequently extended to accommodate both nonperiodic and periodic 3D Coulombic systems [8, 24, 27, 43, 53]. Many different variants of the FMM, including Cartesian-based versions [15, 55], parallel implementations [6, 35], and other efficient implementations, are now available [10, 16, 25, 30, 47, 66]. Some groups have used the fast multipole algorithm in large-scale molecular dynamics simulations (e.g., see [4, 39]).

Recently, *fast* boundary element methods (BEMs) have been developed for solving the Poisson equation (zero ionic strength) for large solvated molecules of arbitrary shapes [3, 44, 70]. In these approaches the fast multipole algorithm for the Coulombic potential is employed to reduce both calculation time and memory demands. Comparable reductions in computational costs can be anticipated in a *fast* BEM implementation for the linear Poisson–Boltzmann equation (PBE). To date, such an implementation has not been realized, however, due to the lack of a fast multipole approximation for the screened Coulombic

potential. A fast boundary element solution of the linear PBE will make it more appealing, especially when coupled to molecular dynamics algorithms for large-scale biomolecular systems.

While FMM and particle–mesh methods are well developed for electrostatic systems governed by the Coulombic potential, no corresponding fast methods are yet available for the Yukawa potential. Hence, computer simulation studies involving this potential have been limited to small systems and employ potential cutoffs to maintain reasonable computational costs [7, 19, 46, 58, 61, 62]. Also, in simulations of supercoiled polyelectrolyte DNA the individual phosphate groups are replaced by charged segments (containing 60 or more phosphate groups), which interact through *approximate* electrostatic pair potentials (e.g., hard-sphere with ionic strength dependent diameter or screened Coulomb) [13, 40, 51, 64] in order to reduce computational costs.

The development of a fast adaptive multipole algorithm for the screened Coulombic potential is therefore crucial to the accurate and computationally efficient modeling of a variety of large-scale Yukawa systems and in the BEM solution of the linear Poisson–Boltzmann equation. In a short communication [36], a parallel FMM algorithm for the Yukawa potential claims to have been developed, but no details of the formulation and implementation are given. An approximate fast adaptive multipole algorithm for the calculation of the Yukawa energy was developed [20] where the $(1/r)$ term was expanded in the conventional manner using a formal Gegenbauer polynomial expansion. To account for ion screening, near-field interactions were treated exactly using Eq. (1) and far-field interactions were simply scaled by $e^{-\kappa r}$, where r is the distance between the expansion point of the inducing group and the evaluation location (either the center of another group or an individual particle). Order of magnitude reductions in CPU times were realized for large ($N = 10^4$) charged systems, and comparison against exact results showed good accuracy (1% energy errors or less). Qualitatively, for small κ, the approximation approaches the Coulombic limit with its well-known accuracy bounds; for large κ, the exponential scaling term dominates beyond a certain range and the higher order multipole terms become less relevant. Though capturing the dominant behavior, this previous approach remains essentially a first-order method where the higher order (dipole, quadrupole, etc.) terms only improve convergence when the product, κr, is small. For large κr, error control is only possible by extending the near-field region.

It is possible to derive a convergent multipole approximation by expanding $(e^{-\kappa r})/r$ as a formal multi-dimensional Taylor series. Unfortunately, as κr increases so does the number of terms required for convergence of the multipole approximation. This behavior is due to the poor convergence of the Taylor series representation of $\exp(-x)$ for large x. To accommodate the screened Coulombic potential, a completely different multipole expansion is warranted. The appropriate multipole expansion is here expressed in terms of spherical modified Bessel functions (SMBFs), the properties of which have been well studied, and for which useful recursion and integral relationships are available. Moreover, the products formed by combining these functions with the spherical harmonics used to describe angular variations can be expressed in terms of minimal polynomials, thereby avoiding the need to convert between Cartesian and spherical coordinates. These products are also amenable to simple recursion relations which facilitate generation of higher order multipoles and formation of spatial gradients.

The layout of the paper is as follows. In the next section (Section 2), the formulation and manipulation of the new SMBF-based method for the Yukawa potential and its gradients are described. Section 3 describes the computer implementation of the fast

adaptive SMBF-based multipole algorithm for the screened Coulombic potential. In Section 4, results are presented illustrating the accuracy of the new SMBF-based multipole expansion for a simple model problem that consists of a single pair of unit positive charges. Timing and accuracy results are also shown for large-scale molecular test systems over a broad range of the Debye–Hückel screening parameter. The molecular systems studied include isolated open linear polyelectrolyte chains, chains of supercoiled and knotted polyelectrolyte DNA, a random distribution of charges inside a cube and a face-centered-cubic (fcc) lattice configuration of charges in aqueous NaCl solutions. Finally, concluding remarks and suggestions for further work are presented in Section 5. Some of the more technical material referred to in the text appears in the appendixes.

2. FAST EVALUATION OF YUKAWA ENERGY AND FORCES

As noted above, the evaluation of the Debye–Hückel potential energy and forces using direct summation entails an $O(N^2)$ operation count due to the long-range interactions between all N charged particles. To reduce this bottleneck, one appeals to fast multipole methods which combine two basic components to reduce the operation count to $O(N \log N)$ or $O(N)$. The first is a hierarchical grouping procedure that assembles the active elements (e.g., charges) into nested groups of specified size. Because of their ability to readily accommodate arbitrary nonuniform charged particle distributions, the adaptive data structures known as octrees [50] are used for this purpose. The second component, which is the primary subject of the present paper, is a multipole approximation to the electrostatic potential and forces induced by a collection of charged particles at sufficiently well-separated, far-field points. The remaining near-field interactions are computed in the conventional manner using direct summation.

To derive a multipole expansion for the screened Coulombic potential valid for all $\kappa \geq 0$, consider (see Fig. 1) a charged source particle located at position, $\underline{\rho}$, and an observation point, $\underline{R}$ (vector quantities are denoted by an underbar). The relative position vector between the source and observation point is $\underline{r} = \underline{R} - \underline{\rho}$ and the distance, $r = |\underline{r}|$. By expressing the position vectors in spherical coordinates, i.e., $\underline{\rho}(\rho, \theta, \phi)$ and $\underline{R}(R, \alpha, \beta)$, a well-known multipole expansion for the Debye–Hückel potential valid for $R > \rho$ is given by [1]

$$\Phi(r, \kappa) = \frac{e^{-\kappa r}}{r} = 8\kappa \sum_{m=0}^{\infty} \hat{I}_{m+1/2}(\kappa\rho)\hat{K}_{m+1/2}(\kappa R) \sum_{k=-m}^{m} Y_{mk}(\theta, \phi)Y^*_{mk}(\alpha, \beta). \qquad (2)$$

The Y_{mk} are the same spherical harmonics employed in the multipole expansion for the Coulombic potential. The asterisk denotes the complex conjugate, and the spherical

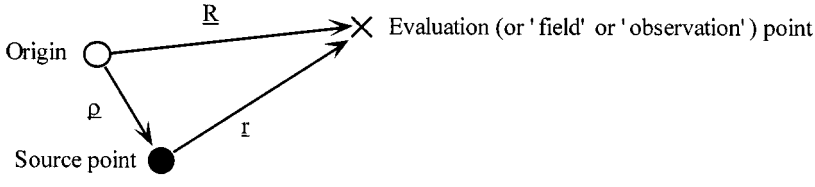

FIG. 1. Schematic showing the location of source and field points relative to the origin of the coordinate system.

modified Bessel functions of the first and third kind are defined as

$$\hat{I}_{m+1/2}(x) \equiv \sqrt{\frac{\pi}{2x}} I_{m+1/2}(x), \qquad \hat{K}_{m+1/2}(x) \equiv \sqrt{\frac{\pi}{2x}} K_{m+1/2}(x), \tag{3a, b}$$

where $I_{m+1/2}(x)$ and $K_{m+1/2}(x)$ are the corresponding conventional (i.e., not spherical) modified Bessel functions of the first and third kinds, respectively. Useful properties of these functions include [1]:

(i) closed form expression in terms of polynomials and an exponential;

(ii) desirable asymptotic behavior for small argument, x:

$$\hat{I}_{m+1/2}(x) \sim \frac{x^m}{1 \cdot 3 \cdot 5 \cdots (2m+1)}, \qquad \hat{K}_{m+1/2}(x) \sim \frac{\pi}{2} \frac{1 \cdot 3 \cdot 5 \cdots (2m-1)}{x^{m+1}}, \tag{4a, b}$$

(iii) efficient evaluation using recurrence relationships among functions of different order.

Because of this last property, only a single exponentiation is required to compute $\hat{I}_{m+1/2}$ or $\hat{K}_{m+1/2}$ for all orders, $m \geq 0$, and hence to evaluate the entire multipole expansion at R.

It is computationally expedient to rescale and combine terms by first defining

$$g_m(x) \equiv \frac{1 \cdot 3 \cdots (2m+1)}{x^m} \hat{I}_{m+1/2}(x), \qquad G_m(x) \equiv \frac{2}{\pi} \frac{x^{m+1}}{1 \cdot 3 \cdots (2m-1)} \hat{K}_{m+1/2}(x) \tag{5a, b}$$

$$\Psi_{mk}(\varrho) = \frac{\rho^m Y_{mk}(\theta, \phi)}{C_{mk}}, \qquad \psi_{mk}(R) = \frac{4\pi}{2m+1} \frac{C_{mk} Y_{mk}(\alpha, \beta)}{R^{m+1}} \tag{6a, b}$$

$$C_{mk} = \sqrt{\frac{(2m+1)(m-k)!(m+k)!}{4\pi}} \tag{6c}$$

and then substituting Eqs. (5) and Eqs. (6) into Eq. (2) to obtain

$$\frac{e^{-\kappa r}}{r} = \sum_{m=0}^{\infty} g_m(\kappa\rho) G_m(\kappa R) \sum_{k=-m}^{m} \Psi_{mk}(\varrho) \psi^*_{mk}(R). \tag{7}$$

This rearrangement is useful in several respects. First, the expansion remains well behaved when $\kappa \to 0$. Then, the small argument behavior of the SMBFs (Eqs. (4a, b) and (5a, b)) reveals

$$\lim_{\kappa \to 0} \frac{e^{-\kappa r}}{r} = \frac{1}{r} = \sum_{m=0}^{\infty} \sum_{k=-m}^{m} \Psi_{mk}(\varrho) \psi^*_{mk}(R), \tag{8}$$

so that the multipole expansion for the Coulombic potential is recovered. This analytical result is also easily reproduced numerically using the rapidly convergent and stable (with respect to round-off) small argument representations of g_m and G_m. The rescalings for the spherical harmonic functions, Eqs. (6), are motivated by the simplified integral expressions for Ψ_{mk} and ψ^*_{mk}, which facilitate development of recursion relationships and evaluation of these functions in Cartesian coordinates (see Appendix A). More importantly, from a computational viewpoint, robust evaluation of the functions g_m and G_m is readily accomplished by slight modification of the SMBF recursion relationships [1].

A useful property of the products,

$$Q_{mk}(\kappa, R) = G_m(\kappa R)\psi^*_{mk}(R), \tag{9}$$

is that their spatial gradients can be expressed as linear combinations of Q_{mk} of different order and degree,

$$\nabla Q_{mk}(\kappa, R) = [A^+_{mk}] \begin{Bmatrix} Q_{m+1,k-1} \\ Q_{m+1,k} \\ Q_{m+1,k+1} \end{Bmatrix} + [A^-_{mk}] \begin{Bmatrix} Q_{m-1,k-1} \\ Q_{m-1,k} \\ Q_{m-1,k+1} \end{Bmatrix}, \tag{10}$$

where the two 3×3 matrices, $[A^{\pm}_{mk}]$ (see Eq. (13) in Appendix B), are *independent* of R (though functionally dependent upon m, k, and κ). The practical consequence of this property is that derivatives of arbitrary order, K, can be readily developed by recursive application of this last relation (simply insert appropriate $(K-1)$-order derivatives on the right-hand side of Eq. (10)). This avoids cumbersome handling of multi-dimensional chain products which would otherwise be required if the gradients of the terms $G_m(\kappa R)$ and ψ^*_{mk} (or $\hat{K}_{m+1/2}(\kappa r)$ and Y_{mk}) were developed separately.

Finally, the combinations $\Psi_{mk}(r)$ and $r^{2m+1}\psi^*_{mk}(r)$ are both m-order polynomials in r. Hence, there is no need to transform to spherical coordinates in order to evaluate these terms. Simple upward recursion relationships can be developed for $\Psi_{mk}(r)$ and $\psi^*_{mk}(r)$ that entail essentially the same computational effort as evaluating the simple m-order Cartesian moments. This is an important observation. Traditionally, multipole expansions of the Coulombic potential have adopted either a Cartesian- or spherical-harmonics-based framework. Key properties of these two approaches are summarized in Table 1. Operating with the quantities Ψ_{mk} and ψ^*_{mk} results in an approach that combines the relative advantages of the pure Cartesian or spherical harmonics representations without forfeiting any desirable properties, as was recently demonstrated by White and Head-Gordon [66]. As in the spherical-harmonics-based approach, multipole expansions to arbitrary order, M, can be developed in a methodical manner and the associated multipole coefficients stored at the minimal $O(M^2)$ cost. However, the square root and circular function evaluations required in converting to spherical coordinates are eliminated. Moreover, local-to-local translation

TABLE 1
Comparison of Cartesian- and Spherical Harmonics-Based Multipole Expansions

Cartesian	Spherical Harmonics
Translation of M-order expansion, $O(M^3)$ using generalized parallel axis theorem	Translation of M-order expansion, $O(M^4)$
Storage for M-order expansion, $O(M^3)$	Storage for M-order expansion, $O(M^2)$
No transcendental function evaluations needed (for Coulombic potential)	At least one square root and one sine operation invoked
Generalization to very high order cumbersome	Arbitrary-order expansions available using simple recursion rules
Difficult to develop arbitrary order derivatives	Arbitrary-order derivatives developed using simple recursion rules

of the multipole coefficients is simply done by recursive application of the binomial theorem along each Cartesian direction. The total cost to shift an M-order expansion is then $O(M^3)$, as compared to $O(M^4)$ for the conventional approach where the shift is performed along all three Cartesian directions simultaneously. Theoretically faster $O(M^2)$ shifting procedures can be effected using fast Fourier transforms and warping operations, but these methods appear quite complicated, particularly if efficiency for low-order expansions is to be preserved [16]. Finally, all spatial gradients of ψ^*_{mk} can be written as linear combinations of $\psi^*_{m'k'}$ of different orders and degrees, m' and k'; no chain product manipulation is necessary to develop arbitrary-order derivatives. Additional details regarding the derivation of the preceding expressions and expressions for the spatial gradients are presented in the appendixes.

3. FAST ADAPTIVE MULTIPOLE ALGORITHM

3.1. *Use of the Multipole Approximation in the Fast Algorithm*

The basic reason for adopting the multipole decomposition is to expedite evaluation of the long range influence of a localized collection of charges, q_α. Summing over charges, α, then from Eq. (7),

$$\sum_\alpha q_\alpha \frac{e^{-\kappa|R-\underline{\rho}_\alpha|}}{|R-\underline{\rho}_\alpha|} = \sum_\alpha q_\alpha \sum_{m=0}^{\infty} g_m(\kappa\rho_\alpha) G_m(\kappa R) \sum_{k=-m}^{m} \Psi_{mk}(\underline{\rho}_\alpha)\psi^*_{mk}(R)$$

$$= \sum_{m=0}^{\infty} \sum_{k=-m}^{m} Q_{mk}(\kappa, R) B_{mk} \tag{11}$$

$$B_{mk} = \sum_\alpha q_\alpha g_m(\kappa\rho_\alpha)\Psi_{mk}(\underline{\rho}_\alpha), \tag{12}$$

where $Q_{mk}(\kappa, R)$ is defined in Eq. (9). This rearrangement implies that the multipole coefficients, B_{mk}, for the entire group can be computed *a priori* and independently from the evaluation point. These coefficients can then be used to approximate the influence of the group at any well-separated evaluation point satisfying $R > \max(\rho_\alpha)$. Therefore, to implement a fast algorithm, one first assembles the interacting elements into a series of hierarchical groups using an octree-based decomposition. The multipole coefficients, B_{mk}, for all groups are then computed by direct summation over charged particles and subsequently used to evaluate all well-separated interactions. Evaluation of the near-field interactions completes the summation procedure.

In the fast implementation of Coulombic interactions, it is usual to first assemble the multipole coefficients upon the finest level (terminal) nodes in the octree by direct summation of individual charges. The multipole coefficients for coarser level nodes are then developed from their finer level counterparts by using shifting theorems or so-called inner-to-inner translation operators rather than by summing over the contained particles. Although this reduces the formal complexity of the multipole construction process from $O(N \log N)$ to $O(N)$, it does not procure significant CPU advantages since the construction of multipole coefficients constitutes a small fraction of total computation time which is dominated by the near-field evaluations and multipole approximation evaluations. When considering the multipole expansions developed for screened Coulombic potentials, the translation operators are considerably more complex and computationally expensive. For example, comparable

translation operators have been developed for the imaginary argument exponential kernel, $\exp(-ikr)/r$ [17, 45, 47]. In the present implementation, the multipole coefficients are computed individually for each box by summing over individual particles. Examination of the CPU times expended in the multipole coefficient construction process has shown them to be insignificant when compared to total calculation times.

A Taylor series approximation can also be invoked to reduce the formal complexity of the algorithm from $O(N \log N)$ to only $O(N)$ (this estimate ignores octree construction which remains $O(N \log N)$ but usually requires negligible CPU time). The basic idea is to extrapolate or project far-field electrostatic contributions that have been accumulated for a parent group to each of its immediate descendant groups or, if no such groups exist, to the individual elements contained in the group. Denote by vector $\underline{b}$ the relative position between the centers of a pair of nested groups or between an individual charge and the center of the group it is contained in and consider the evaluation of Eq. (11) at location $\underline{R}+\underline{b}$, where $|\underline{R}+\underline{b}| > \max(\rho_\alpha)$ and $b < R$. Under these conditions, each of the terms in the expansion, Eq. (11), can be approximated by a truncated Taylor series,

$$Q_{mk}(\kappa, \underline{R}+\underline{b}) \cong Q_{mk}(\kappa, \underline{R}) + \underline{b}\cdot\frac{\partial}{\partial \underline{R}} Q_{mk}(\kappa, \underline{R}) + \frac{1}{2}\underline{b}\cdot\left[\frac{\partial^2}{\partial \underline{R}^2} Q_{mk}(\kappa, \underline{R})\right]\cdot\underline{b} + \cdots, \quad (13)$$

where the successive gradients are obtained using Eq. (10).

It should be pointed out that in order to preserve the improved convergence behavior afforded by the SMBF-based multipole expansion, the Taylor series extrapolation procedures should be replaced with multipole translation operators which are more efficient (when using diagonal forms of these operators [17, 45, 47]) and more accurate for $\kappa|\underline{b}| \gg 1$. In the Coulombic case there is a close correspondence between the multipole and Taylor series approximations. Both the multipole coefficients and the translation operators used to shift the expansions downward from coarser to finer level boxes can be formally derived from a multi-dimensional Taylor series representation of the $1/r$ kernel. For the screened Coulombic potential, the Taylor series converges very slowly for $\kappa R \gg 1$, which motivated the SMBF-based multipole expansion in the first place. For similar reasons, translation operators for SMBF-based multipole expansions are likely to converge more uniformly with κ than the Taylor series extrapolation procedures described above. Such translation operators can be derived using the same procedures developed for FMM solutions to the 3D Helmholtz [17, 45, 47]. This has not yet been implemented, however, and the current Taylor series-based extrapolation may exhibit κ-dependent convergence behavior, though in the cases considered, the actual errors have remained quite small. An option is available to dispense with the Taylor series extrapolation and perform the analysis using only the multipole approximation applied to the individual evaluation points. The resulting operation count for N particles is then $O(N \log N)$, which still constitutes a "fast algorithm," and the error can be fully controlled by adjusting the order of the multipole expansion. In practice, the computation time for the $O(N \log N)$ algorithm increases by approximately a factor of 2 to 4.

3.2. *Construction of Groups*

The final remaining issue is how to form the groups and distinguish between near- and far-field interactions. In this regard, the fast algorithm closely resembles established fast adaptive multipole methods using octree decompositions. Beginning with a single cube

encompassing the domain of interest, particles are inserted in succession. At any point, the octree consists of a hierarchy of cubes or boxes obtained by recursively dividing the original cube. As a new particle is inserted, one first conducts a downward search through the octree to establish the terminal (smallest) box, ib, containing the particle. If, upon addition of the new particle, the total number of particles within this cube exceeds a specified threshold, the cube is divided into eight "child" boxes and the particles contained in ib are reassigned to the newly created boxes. This procedure continues until all particles have been inserted.

Five types of interactions are possible between a pair of boxes according to the combinations of multipole and/or Taylor series approximations that may be invoked. If L_s is a separation parameter used to distinguish between near-/far-field regions; d_s and d_f are the side lengths of the source (inducting) and field (observation) boxes, respectively; and D_{sf} is the separation distance between the source and field boxes (i.e., the smallest distance between the perimeters of these boxes), then five different interaction types may be distinguished:

(i) direct interaction: interactions between particles in these boxes must be summed directly;

(ii) multipole expansion only: $L_s d_s \le D_{sf} < L_s d_f$;

(iii) Taylor series expansion only: $L_s d_f \le D_{sf} < L_s d_s$;

(iv) both multipole and Taylor series expansions: $D_{sf} \ge L_s \max\{d_f, d_s\}$;

(v) no interaction: the inducting effects were already contained within the interactions between ancestors of the source and field boxes.

Figure 2 depicts these interaction types for the case $L_s = 1$.

3.3. *Overall Assembly of Fast Energy and Force Calculation*

The fast computation of the screened Coulombic energy, U_e, for a collection of N charged particles, i, is assembled as follows. First, an octree is developed about the configuration of charged particles and used to define the hierarchical groups—each group is composed of the particles in a particular box or cell of the octree. The pointer structures needed to identify

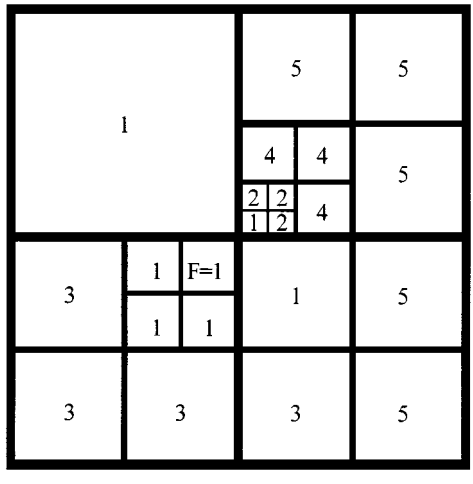

FIG. 2. Two-dimensional example illustrating the five types of interactions with a field box, F. Only terminal (leaf) boxes are shown and $L_s = 1$ is assumed. The letters correspond to the interactions described in the text (See Section 3.2).

the particles contained in a given box are also developed at this stage. Next, the multipole coefficients, B_{mk}, for each group are computed according to Eq. (12). This completes the "upward" pass of the fast evaluation process.

The downward pass proceeds differently according to whether Taylor series extrapolations are invoked or not during this stage. The search is simpler if no Taylor series extrapolations are invoked. In this case, the total screened Coulombic energy is evaluated by expressing

$$U_e = \frac{1}{2\varepsilon} \sum_{i=1}^{N} q_i u_i \tag{14}$$

and decomposing

$$u_i = \sum_{j \neq i} \frac{q_j e^{-\kappa r_{ij}}}{r_{ij}} \cong \sum_{j \neq i,\, j \in N_i} \frac{q_j e^{-\kappa r_{ij}}}{r_{ij}} + \sum_{jg} \sum_{m=0}^{M} \sum_{k=-m}^{m} Q_{mk}(\kappa, R_i)(B_{mk})_{jg}, \tag{15}$$

where N_i is the set of points, j, considered near-field to point, i, and jg are the far-field groups containing the remaining points, $j \notin N_i$, whose contributions are evaluated using the multipole approximation. Forces, $\underline{f}_i = -(q_i/\varepsilon)\partial u_i / \partial R_i$, may be similarly decomposed:

$$\underline{f}_i \cong q_i \sum_{j \neq i,\, j \in N_i} \frac{q_j e^{-\kappa r_{ij}}(1 + \kappa r_{ij})}{\varepsilon r_{ij}^3}(R_i - R_j) - \frac{q_i}{\varepsilon} \sum_{jg} \sum_{m=0}^{M} \sum_{k=-m}^{m} \nabla Q_{mk}(\kappa, R_i)(B_{mk})_{jg} \tag{16}$$

(note that the coefficients, B_{mk}, are treated as constants during the differentiation). The evaluation of each u_i and $\underline{f}_i$ then entails a top-to-bottom search through the octree. Starting with the root cell encompassing the entire domain, descendant cells, *jg*, are recursively searched to see whether a multipole approximation may be applied. If so, the multipole evaluation is made and the search through further descendants pruned at this cell. Otherwise, the search continues through the descendants of *jg*. If no further descendants exist, then the contributions from the individual particles, j, in the cell are near-field and must be evaluated directly.

When Taylor series extrapolation is invoked, a pre-order traversal [50, 54] of the octree is carried out which ensures that every cell in the octree is visited before its subdivided descendant cells. For each visited cell, *ig*, the tests of Section 3.2 are applied and the necessary near- and/or far-field interactions carried out. If the cell contains further descendants, then the accumulated contributions to u_{ig} and $\underline{f}_{ig}$ (Eqs. (15) and (16) evaluated at the center of cell, *ig*) are transferred to the centers of these descendant cells using the Taylor series extrapolation, Eq. (13). Otherwise, if cell *ig* is terminal and has no descendants, then the Taylor series extrapolation is applied to the individual particles contained in cell *ig*. The remaining near- and far-field interactions for these individual particles are then carried out, thus completing the evaluation of u_i and $\underline{f}_i$.

4. RESULTS AND DISCUSSION

4.1. *Simple Test of the SMBF-Based Multipole Expansion*

In order to assess the accuracy of the new SMBF-based multipole expansion, a simple model problem containing a pair of unit charges is considered. The source charge is placed

at unit radius, $r_s = 1$, from the origin and the multipole coefficients about the origin are computed. The fourth-order multipole expansion is then evaluated at a series of field points located at different radial distances from the origin, r_f. For each such radius, r_f, the field point vector is rotated (i.e., the spherical angles are varied) and the maximum relative electrostatic energy error,

$$e_{\max}(r_f) = \max_{\alpha,\beta}\left\{ \frac{E_{\text{multipole}}(r_f) - e^{-\kappa r}/r}{1/r} \right\}, \tag{17}$$

is recorded. Here, $r = |R_f - R_s|$ and α, β are the spherical angles of the field point. Note that the electrostatic energy error is normalized by $1/r$ (the Coulombic potential), which is more useful at large κ since the screened Coulombic energy is then effectively short-range and becomes negligible beyond $r > 7/\kappa$.

It is also of interest to study what transpires when one retains the conventional multipole expansion for the Coulombic potential and simply scales this approximation by $\exp(-\kappa r_f)$. Referring to this as the "scaled Coulombic" approximation [20], one anticipates low errors at both sufficiently small and sufficiently large values of κ.

The variation in $e_{\max}$ with r_f and κ is depicted in Fig. 3. Note that the results from the "scaled Coulombic" approximation (Fig. 3a) and SMBF-based multipole expansion (Fig. 3b) are plotted on identical scales. As shown in Fig. 3a, for the "scaled Coulombic" approximation, the relative electrostatic energy error is seen to increase rapidly with κ and to persist well into the far-field region $r_f > r_s$. The maximum relative electrostatic energy error occurs roughly in the range $0.5 < \kappa < 0.7$; beyond this range the electrostatic energy error decays rapidly with r_f. In contrast, the results obtained using the SMBF-based multipole expansion exhibit much tighter energy error control at all κ (see Fig. 3b). It is evident that all relative electrostatic energy errors lie below the curve corresponding to $\kappa = 0$ so that, unlike the previous case, the relative electrostatic energy error reduces monotonically with both r_f and κ. A corollary is that useful error bounds can be developed for the present approximation based upon the well-known results for the Coulombic case. In particular, the estimate for the maximum error in a pure Coulombic M-order multipole expansion, $e_{\max} \sim (r_s/r_f)^{M+1}$, carries over to the SMBF-based multipole approximation. Though not shown here, it can also be demonstrated that the maximum relative electrostatic energy error decays rapidly with the order of the multipole expansion, M, which can therefore be used as means of controlling overall solution tolerance. The improved and predictable convergence behavior of the SMBF-based multipole expansion for all $\kappa \geq 0$ favors its use for the calculation of screened Coulombic electrostatic interactions in large molecular charged systems.

4.2. *Performance and Accuracy of the Fast Adaptive Multipole Algorithm*

The computational performance of the new fast adaptive multipole algorithm (implemented in FORTRAN 77) was examined for several model finite systems involving both uniform and nonuniform charge distributions and different salt concentrations. The systems studied include interwound, knotted, and lobed DNA configurations [51, 52], and open linear polyelectrolyte chains containing up to 10,000 charged particles. Also, a face-centered-cubic lattice configuration of unit charges with a fixed reduced density of 0.7 was considered. Finally, computational studies involving up to 103,823 charged particles randomly distributed inside a cube were performed.

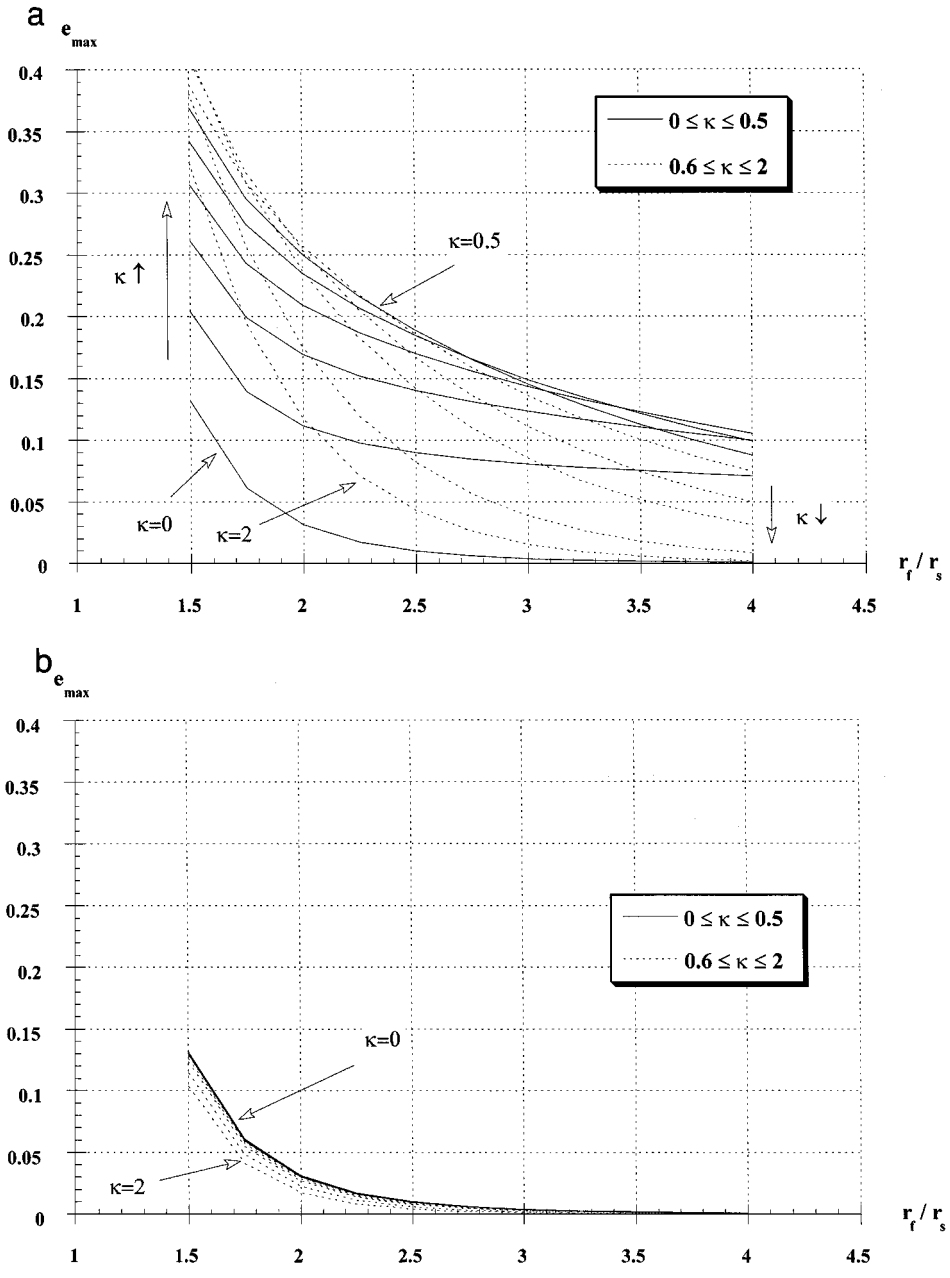

FIG. 3. Variation of the maximum relative electrostatic energy error, $e_{\max}$ (defined in Eq. (17) of the text), with separation ratio, r_f/r_s (r_f and r_s are the distances from the origin of the field and source positions, respectively), and Debye–Hückel screening parameter, κ, using (a) the "scaled Coulombic" approximation and (b) the four-order ($M = 4$) SMBF-based multipole expansion.

Unless otherwise stated, all the results reported below were obtained using the following fixed input parameters: the maximum number of particles per terminal node in the octree, $N_c = 12$ (nodes that contain more than N_c particles are subdivided into "child" nodes); the box separation parameter, $L_s = 1$; and the order of the multipole expansion, $M = 2$.

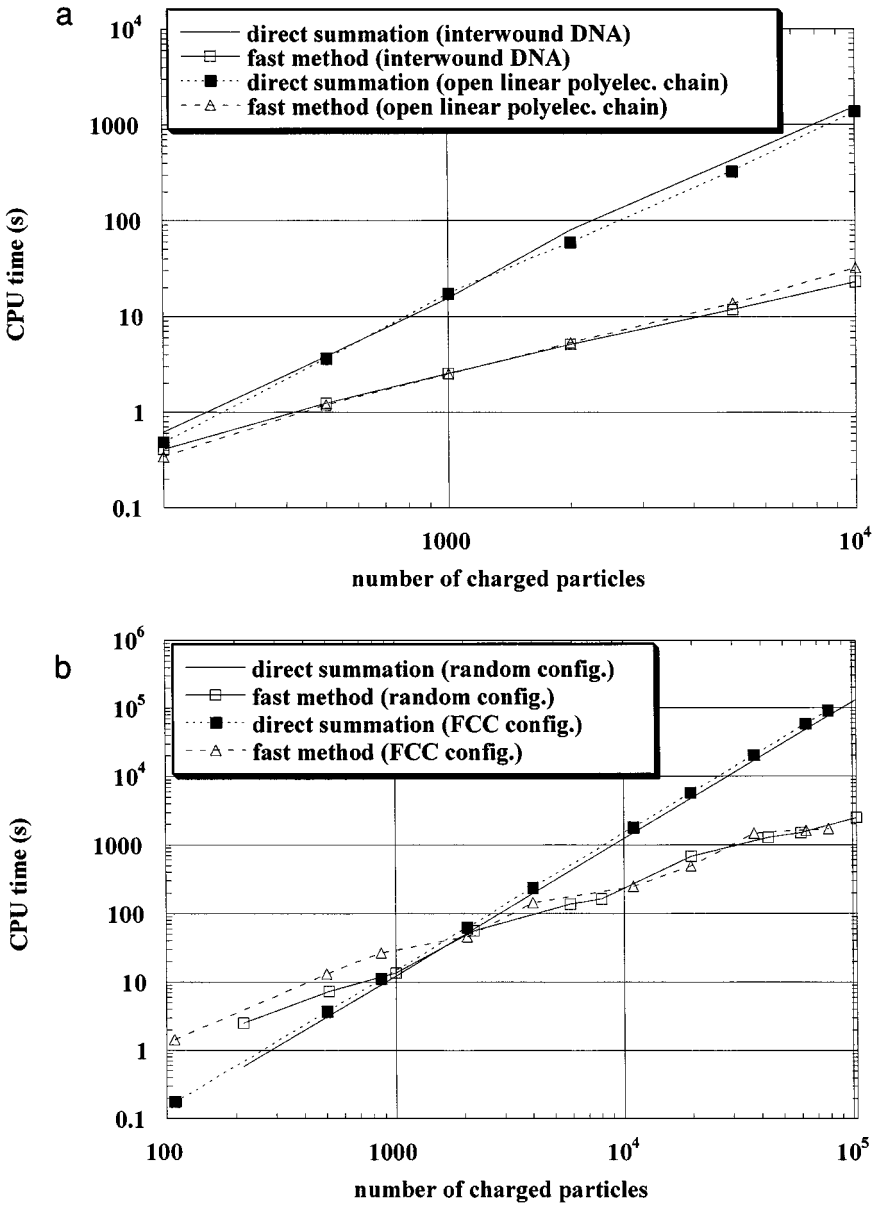

FIG. 4. Comparison of the CPU time (in seconds) as a function of the number of charged particles involved in the calculation of the electrostatic energy and forces of an interwound DNA chain and open linear polyelectrolyte chain (a) and fcc lattice and random configuration of charges (b) at 0.1 M NaCl, using the direct and fast summation methods.

4.2.1. Timing. Timings for the calculation of the Yukawa energy and forces using both direct and fast adaptive multipole algorithm were obtained using a 100-MHz single processor (R40000) SGI workstation. Because of the lengthy computation times, CPU estimates for direct summation applied to systems involving more than 11,000 particles were estimated by extrapolation.

Figure 4a compares the CPU time required to compute the electrostatic energy and forces for open linear polyelectrolyte chains and supercoiled polyelectrolyte DNA chains

at 0.1 M NaCl using the direct and fast summation methods. The computational merits in adopting the fast over direct summation algorithm are clearly evident. Examination of the curves confirms that the direct summation computation exhibits the expected quadratic time complexity, whereas the CPU time of the fast summation method scales as $O(N^{1.14})$ and $O(N^{1.02})$ for the open chains and supercoiled DNA chains, respectively. The nearly linear scaling of the fast method is essentially independent of both the assumed chain configuration and salt concentration. Figure 4b reports CPU times for the fcc and random configuration of charges at 0.1 M NaCl. The asymptotic scalings obtained with the fast method are now $O(N^{1.06})$ for the fcc lattice configuration and $O(N^{1.14})$ for the random charge distributions. These estimates are very similar to those obtained for the polyelectrolyte chains and confirm that the asymptotic CPU scalings of the fast method are essentially independent of salt concentration and charged particle configuration.

In the application of fast summation methods, the leading constant in the asymptotic CPU behavior also assumes practical importance and is found to be configuration-dependent. Figure 5 shows the relative computation speedup obtained when using the fast algorithm in lieu of the direct summation method. The results reflect the dependence upon the basic dimensionality of the structure—the highest speedup factors are obtained for the essentially chainlike arrangements (e.g., polyelectrolyte molecules) and the lowest values for the volumetric charged particle distributions (e.g., fcc lattice and random charge distributions). The crossover point where the fast method proves faster than the direct summation method is ∼200 for the polyelectrolyte chains and ∼2000 for the fcc lattice and random particle distributions. Greengard and Rokhlin [24] observed similar behavior for the FMM applied to Coulombic potentials, where the crossover points occurred using 100 and 1000 particles for the 2D and 3D charged particle systems, respectively. These results are qualitatively explained by noting that the number of near-field interactions is proportional to the number of surrounding boxes that are populated by particles. For a D-dimensional charged

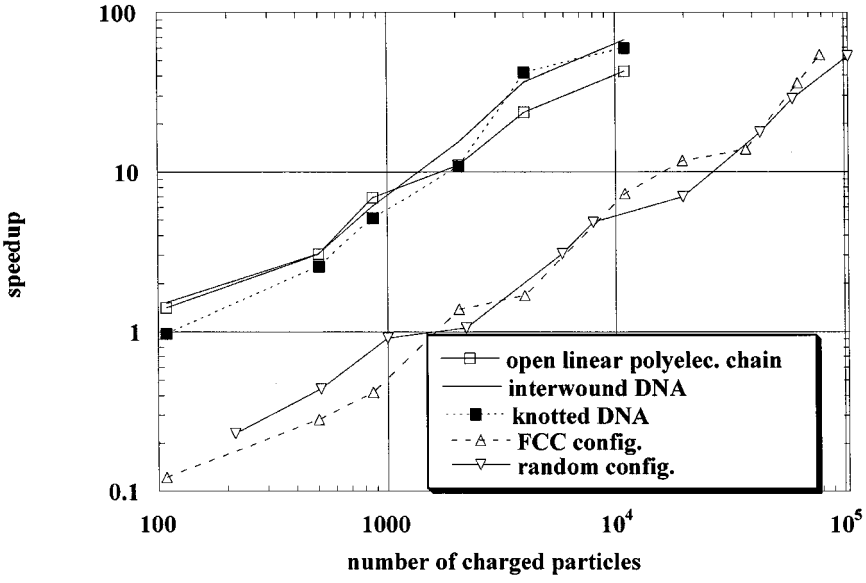

FIG. 5. Plot of the speedup of the fast method relative to the direct method versus the number of charged particles in different charged systems: interwound DNA, knotted DNA, open linear polyelectrolyte chain, fcc lattice, and random configuration of charges at 0.1 M NaCl.

particle arrangement (where $D = 1$, 2, and 3 refers to essentially chainlike, surfacelike, and fully 3D particle distributions, respectively), the number of such near-field boxes is roughly $(2L_s + 1)^D$. This agrees with the observed one order of magnitude disparities in speedup for the one- and three-dimensional structures computed using $L_s = 1$. For essentially 2D structures associated with solvated biomolecular surfaces in BEM formulations of the linear Poisson–Boltzmann equation one anticipates speedups that are roughly one-third those for the 1D structures considered here.

4.2.2. Accuracy. The advantages realized in terms of computation time when adopting the fast algorithm must be weighed against the accompanying errors incurred in truncating the infinite multipole expansion. It is important to point out that this truncation error has two properties that must be considered in practical applications. The first is the magnitude of the error, which is of direct and obvious importance to the user when interpreting results and assessing overall accuracy. The second property, which is not dealt with here, concerns the discontinuous behavior of the error with respect to configurational changes. Consider a deterministic optimization process where a minimum energy configuration of, say, a supercoiled DNA chain is sought under the simultaneous action of elastic and electrostatic forces. During the optimization process, the locations of the charged particles change so that they will be reassigned to different cells in the octree (the octree itself will usually be regenerated periodically). The multipole approximation to the long-range influence of a charged particle that has been reassigned to a new cell changes discontinuously, which can pose difficulties for gradient-based optimization algorithms. Also, energy drifts observed in a molecular dynamics simulation of a 36,000-atom protein–DNA–water system, which employed a high-order FMM algorithm for the Coulombic forces, were attributed to similar discontinuous behavior of the multipole expansion approximation [5]. Increasing M or L_s can reduce these discontinuities, but this is an inefficient way to proceed because numerical smoothness rather than absolute error requirements then dictate the order of the multipole expansion. To our knowledge, this problem has not been addressed, and the ability to perform deterministic optimization and molecular dynamics using low-order multipole expansions remains an important and useful objective.

In the present study, the dependence of the electrostatic energy and force errors upon salt concentration and various computational parameters, including L_s and M, is assessed. Accuracy is measured in terms of the relative electrostatic energy error, $(E_{\text{approx}} - E_{\text{exact}})/E_{\text{exact}}$, and the relative root-mean-square (rms) electrostatic force error, $\|\mathbf{f}_{\text{approx}} - \mathbf{f}_{\text{exact}}\|/\|\mathbf{f}_{\text{exact}}\|$, where E_{approx} is the approximate electrostatic energy using the fast method; E_{exact} is the exact energy obtained by direct summation; $\mathbf{f}_{\text{approx}}$ and $\mathbf{f}_{\text{exact}}$ are the $(3N)$-vector of concatenated charged particle forces computed using the fast and direct summation techniques, respectively; and $\|\cdot\|$ is the Euclidean norm.

Table 2 presents the electrostatic energy and force errors of several charged systems over a broad range of salt concentration. As is evident from Table 2, the electrostatic energy error is at most 0.002 for all charge configurations considered and remains essentially independent of salt concentration. The electrostatic force errors (Table 2) are also insensitive to salt concentration up to 0.01 M NaCl, but are at least an order of magnitude larger than the electrostatic energy errors. The dependence of the electrostatic energy and rms force error upon system size at fixed salt concentration (0.1 M NaCl) is shown in Table 3. The variation of energy error with system size is configuration dependent, but much less so for the rms force error.

TABLE 2

Electrostatic Energy Error and Root-Mean-Square (rms) Electrostatic Force Error for Different Configurations of Charged Particles under Varying NaCl Concentrations

Configuration	NaCl concentration (M)	Energy error	rms force error
Open linear polyelectrolyte chain	1.0×10^{-6}	3.7×10^{-4}	9.4×10^{-3}
	1.0×10^{-4}	2.0×10^{-4}	8.9×10^{-3}
	1.0×10^{-2}	1.9×10^{-4}	4.8×10^{-3}
	1.0×10^{-1}	4.6×10^{-5}	1.3×10^{-3}
	1.0	1.0×10^{-6}	5.9×10^{-5}
Interwound DNA	1.0×10^{-6}	6.7×10^{-4}	1.8×10^{-1}
	1.0×10^{-4}	5.1×10^{-4}	1.9×10^{-1}
	1.0×10^{-2}	3.4×10^{-4}	2.3×10^{-1}
	1.0×10^{-1}	2.1×10^{-4}	1.2×10^{-1}
	1.0	1.1×10^{-5}	1.3×10^{-2}
Random charge distribution inside a cube	1.0×10^{-6}	2.8×10^{-4}	1.2×10^{-2}
	1.0×10^{-4}	3.0×10^{-4}	1.2×10^{-2}
	1.0×10^{-2}	1.6×10^{-4}	1.5×10^{-2}
	1.0×10^{-1}	1.0×10^{-3}	2.2×10^{-2}
	1.0	7.4×10^{-4}	7.7×10^{-3}
Face-centered-cubic lattice	1.0×10^{-6}	2.4×10^{-4}	1.2×10^{-2}
	1.0×10^{-4}	2.7×10^{-4}	1.3×10^{-2}
	1.0×10^{-2}	3.3×10^{-4}	1.3×10^{-2}
	1.0×10^{-1}	3.1×10^{-6}	1.9×10^{-2}
	1.0	2.0×10^{-3}	5.0×10^{-2}

TABLE 3

System Size Dependence of the Electrostatic Energy Error and Root-Mean-Square (rms) Electrostatic Force Error for Different Configurations of Charged Particles at 0.1 M NaCl

Configuration	Number of charged particles	Energy error	rms force error
Open linear polyelectrolyte chain	500	1.9×10^{-5}	6.8×10^{-4}
	1,000	7.7×10^{-5}	7.3×10^{-4}
	2,000	2.2×10^{-5}	1.1×10^{-3}
	5,000	4.7×10^{-5}	1.4×10^{-3}
	10,000	4.6×10^{-5}	1.3×10^{-3}
Interwound DNA	500	5.4×10^{-4}	3.0×10^{-2}
	1,000	2.7×10^{-4}	3.7×10^{-2}
	2,000	2.8×10^{-4}	8.0×10^{-2}
	5,000	2.2×10^{-4}	1.0×10^{-1}
	10,000	2.1×10^{-4}	1.2×10^{-1}
Random charge distribution inside a cube	500	7.5×10^{-5}	1.6×10^{-2}
	1,000	3.6×10^{-4}	1.7×10^{-2}
	2,000	6.4×10^{-4}	2.0×10^{-2}
	5,000	1.0×10^{-3}	1.9×10^{-2}
	10,000	1.0×10^{-3}	2.2×10^{-2}
Face-centered-cubic lattice	500	3.1×10^{-4}	9.7×10^{-3}
	1,000	3.6×10^{-4}	1.1×10^{-2}
	2,000	1.3×10^{-4}	1.3×10^{-2}
	5,000	2.1×10^{-4}	1.6×10^{-2}
	10,000	3.1×10^{-6}	1.9×10^{-2}

There are two possible reasons for the relatively high electrostatic rms force errors. First, the net electrostatic forces are inherently more sensitive to errors because their evaluation involves cancellation of equal and opposite contributions. Consider, for example, a circular arrangement of equal charges and evaluate the net force at a particle, i, located at azimuthal angle $\theta = 0$. From symmetry the force component in the circumferential direction, f_θ is zero and only a radial component, f_r, remains. Now f_θ can be decomposed into two components, $f_{\theta L}$ and $f_{\theta R}$, representing the respective contributions of particles located between azimuths, $\theta \in [-\pi, 0]$ and $\theta \in [0, +\pi]$. For large particle counts, one can show that the magnitudes of the two components, $f_{\theta L}$ and $f_{\theta R}$, are much larger than the net residual forces, f_r and f_θ, so that multipole errors that are small compared to $f_{\theta L}$ are nevertheless large compared to f_θ and f_r. The second reason for higher force errors is that setting $L_s = 1$ leads to slowly converging multipole series. This is discussed further below.

The order of the multipole expansion, M, and the separation criterion, L_s, are the primary parameters available for controlling error. In its current form, the software accommodates arbitrary-order multipole expansions. However, the Taylor series extrapolations used to project accumulated energy and force contributions from coarser to finer level cells are limited to second order. For fast calculations of systems governed by Coulombic potentials, the error is controlled by the minimum expansion order adopted in the multipole and Taylor series approximation, and it is therefore usual to use the same order in both approximations. This also applies to the Debye–Hückel interactions, as can be inferred from the results in Figs. 6a and 6b depicting the energy and force errors for the random distribution of 8000 charged particles. Results were obtained using: (i) both multipole and Taylor series approximations of order, $M = 2$; (ii) a multipole expansion of order, $M = 4$, and a second-order Taylor series extrapolation; (iii) $M = 2$ multipole expansions alone; and (iv) $M = 4$ multipole expansions alone. When both multipole and Taylor series expansions are employed (cases (i) and (ii)), convergence stalls for $M > 2$. This is dramatically clear in Fig. 6b, where increasing M from 2 to 4 has practically no effect since the overall rms force error is now controlled entirely by the order of the Taylor series extrapolation, which is 2 in both cases. When only the multipole expansion is employed (cases (iii) and (iv)), the errors reduce with M in the predictable way with at least a fivefold reduction in the rms force error when doubling the multipole expansion order. Similar behavior in the energy and rms force errors is obtained for the other charge configurations, which suggests the need for higher order Taylor series expansions accompanying same order multipole expansion approximations. On the other hand, the use of higher order multipole expansions increases the cost involved in their evaluation, and it remains unclear at what point (or, rather, for which problem size) the combination of higher order multipole and Taylor series expansions with nearly $O(N)$ asymptotic behavior outperforms the $O(N \log N)$ scalings procured using multipole expansions alone.

The rms force errors recorded in Fig. 6b can be rapidly reduced by increasing the box separation parameter, L_s. Indeed, careful examination of the error bounds associated with the multipole expansion for the Coulombic potential [49] reveals that although setting $L_s = 1$ ensures convergence to the exact value, the convergence rate can be slow, particularly when the L_∞ norm is used to define the distance, D_{sf}, between a pair of source and field boxes. This is because the error bounds are properly formulated in terms of minimum enclosing spheres rather than cubes, which implies that the maximum errors in the multipole expansion for a cell with side d evaluated at distance R from the center behave as $(\sqrt{3}d/2R)^{M+1}$ rather than

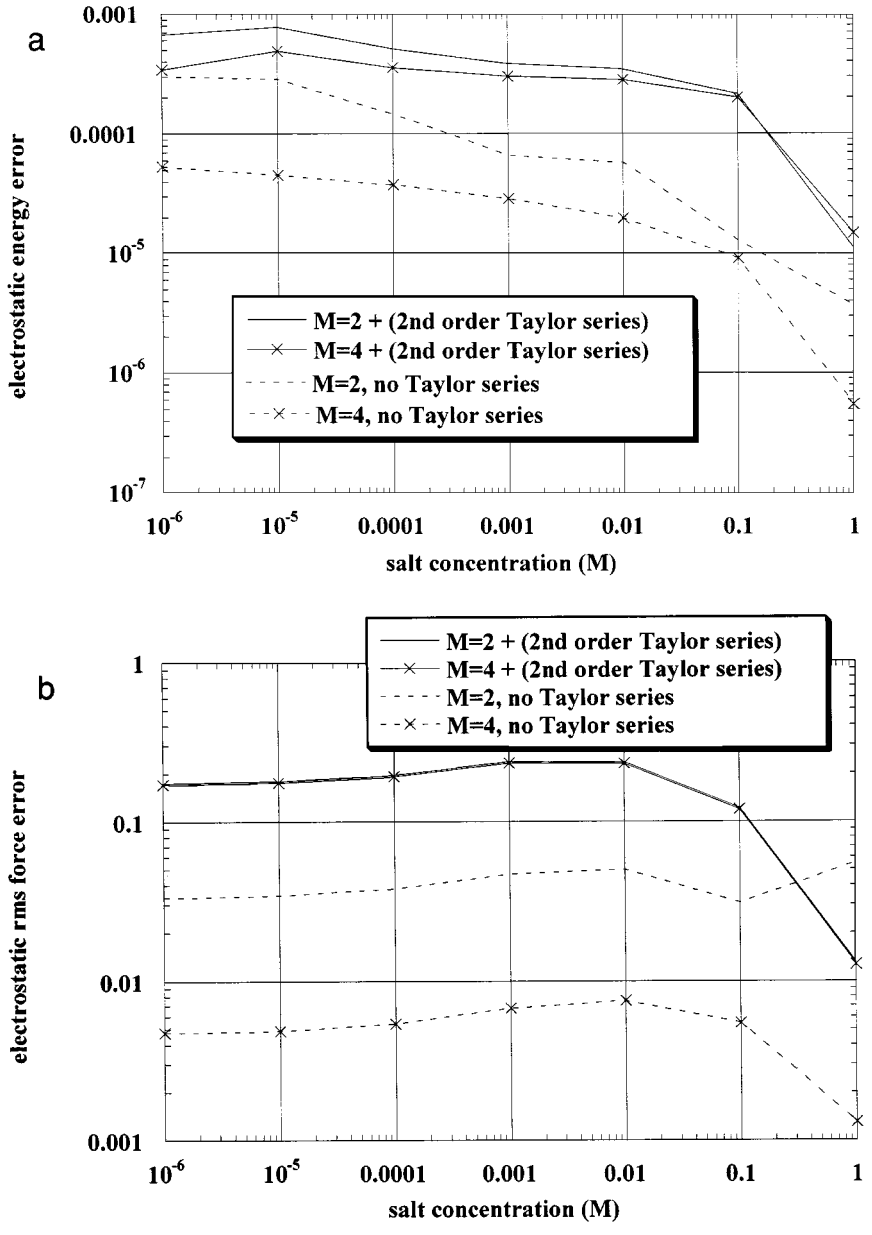

FIG. 6. Dependence of the (a) electrostatic energy error and (b) electrostatic rms force error of the random distribution of 8000 charges, over a broad range of salt concentration, on the order of the multipole expansion, M, when only the M-order multipole expansion is invoked or both M-order multipole and second-order Taylor series expansions are employed.

$(d/2R)^{M+1}$. For $L_s = 1$, $d/R < 2/3$ and so the truncation error $\sim 0.577^{M+1}$. For $L_s = 2$, the error obeys a more favorable 0.346^{M+1} behavior.

Figure 7 shows the dependence of the electrostatic energy and force error for the random distribution of 8000 charged particles upon L_s. As expected, both errors decrease with L_s and order of magnitude reductions are observed at all salt concentrations when incrementing L_s from 1 to 2. Similar behavior is observed for the other charge configurations. The improved

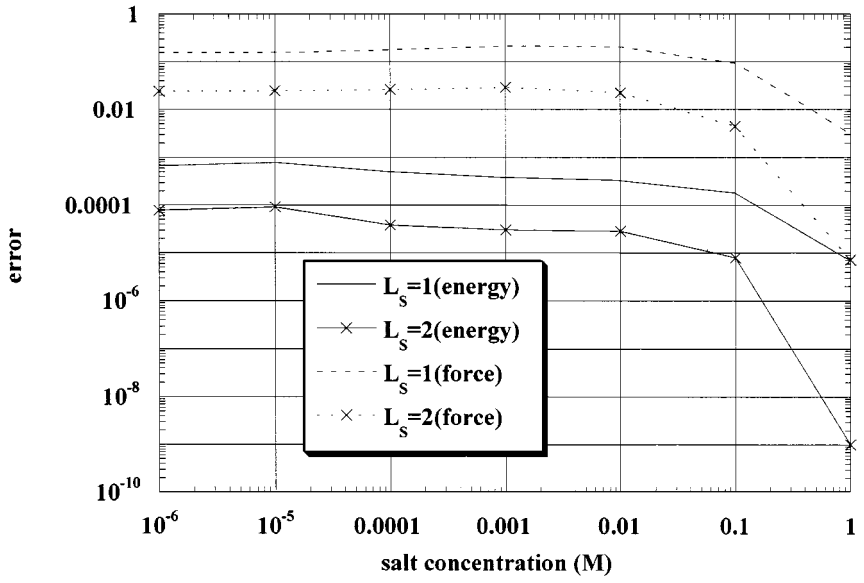

FIG. 7. Dependence of the electrostatic energy and rms force errors for the random distribution of 8000 charges on the separation criterion, L_s, over a broad range of salt concentration.

accuracy is accompanied by longer calculation times—increasing L_s from 1 to 2 typically incurs a factor of 2 to 3 increase in computation time. These results show that considerable benefit in terms of reduced computation time and enhanced accuracy can be derived by directing careful attention to the tests (and distance norms) used to distinguish between near- and far-field interactions. Close scrutiny of these tests is imperative when considering interacting elements of finite size (e.g., boundary elements) since the multipole expansion may not converge at all unless the element size is accounted for. The authors are currently developing tests based upon minimum enclosing spheres.

5. CONCLUSIONS AND FUTURE WORK

A new multipole expansion using spherical modified Bessel functions has been developed for the rapid calculation of electrostatic interactions with implicit ion screening. A key advantage of the SMBF-based multipole expansion for the Debye–Hückel kernel is that the number of multipole terms necessary to attain a given accuracy is essentially independent of κ. Detailed studies involving a single source particle show that the maximum relative electrostatic energy error incurred by an M-order multipole expansion of the Yukawa potential is bounded above by the error of the equivalent multipole expansion for the Coulombic potential. Also, the relative energy error decreases monotonically with both the distance of the evaluation point, $r_f > r_s$, and the Debye screening parameter, κ.

A fast adaptive multipole algorithm was developed by combining the new SMBF-based multipole expansion with an octree-based hierarchical grouping procedure. This algorithm is shown to achieve nearly $O(N)$ scaling in the computation of the screened Coulomb energy and forces irrespective of charged particle configuration and fixed salt concentration. The leading constant in the asymptotic CPU behavior is influenced by

several parameters, including the configuration of charged particles. In particular, an order of magnitude difference in CPU times is observed when considering essentially 1D, chainlike structures (e.g., polyelectrolyte chains) compared to fully 3D arrangements such as fcc lattice and random charge configurations. The accuracy in the screened Coulombic energy and force computation can be effectively controlled by adjusting the number of terms retained in the multipole expansion, M, and the box separation parameter L_s.

Recommendations for future research efforts should emphasize both the theoretical aspects of the SMBF-based multipole expansion and the practical implementation issues. For example, fast summation algorithms developed for pure Coulombic potentials make extensive use of translation theorems to shift multipole expansions between different locations. Though comparable results can be developed for the multipole expansions of screened Coulomb potentials (such results are derived from expressions for the $\exp(-ikr)/r$ kernel, see Refs. [17, 45, 47]), the theory is not as well developed and the shifting operations are considerably more expensive. It would also be of both theoretical and practical interest to conduct a more rigorous error bound analysis of the new SMBF-based multipole expansion. Tighter error bounds can be employed to produce more efficient fast multipole algorithms [42]. The new fast adaptive multipole algorithm is amenable to parallel operation and work is presently being pursued by the authors to develop a parallel version of the method using the MPI communication protocol.

Coupling the present fast adaptive multipole algorithm to existing MC and MD codes will allow simulation of large-scale systems, such as weakly charged polyelectrolyte chains and polyelectrolyte supercoiled DNA, whose electrostatic interactions can be well described by the Debye–Hückel potential. Finally, the authors are currently involved in incorporating the fast algorithm into a boundary element code to solve the linear Poisson–Boltzmann equation for large solvated biomolecules. In boundary element methods, storage considerations rather than CPU concerns usually impose limits upon problem size, and a major reason for using a fast summation algorithm is to alleviate storage as well as CPU costs. Results from this endeavor will be presented elsewhere.

APPENDIX A

Spherical Harmonics Expressed in Cartesian Coordinates

It is well known that the products $r^n Y_{nm}$ can be expressed as multi-dimensional polynomials in Cartesian coordinates [1, 41]. To develop such expressions as well as relations for the spatial derivatives of such functions and identities between spherical harmonics of different orders and degree the following result proves useful. Begin by defining the complex quantity,

$$W = z + i\{x\cos u + y\sin u\} = z + i\{qe^{iu} + pe^{-iu}\}, \tag{A.1}$$

where

$$p = \frac{x+iy}{2},\ q = \frac{x-iy}{2} \qquad \Rightarrow \qquad x = p+q,\ y = i(q-p); \tag{A.2}$$

then the integral

$$\Psi_{nm} = \frac{i^m}{2\pi n!} \int_0^{2\pi} W^n e^{imu}\, du \tag{A.3}$$

is related to the products

$$r^n Y_{nm} = C_{nm} \Psi_{nm}, \qquad C_{nm} = \sqrt{\frac{(2n+1)(n-m)!(n+m)!}{4\pi}}, \tag{A.4a, b}$$

where Y_{nm} is the normalized spherical harmonic function.

Noting

$$\int_0^{2\pi} e^{iku}\, du = \begin{cases} 2\pi, & k = 0 \\ 0, & k \neq 0 \end{cases}, \tag{A.5}$$

Eq. (A.3) reduces to the simple form

$$\Psi_{nm} = \sum_{k=0}^{[(n-m)/2]} \frac{z^{n-m-2k}}{(n-m-2k)!} \frac{q^k}{k!} \frac{(-p)^{m+k}}{(m+k)!}, \tag{A.6}$$

where $[*]$ denotes the rounded down integral component of the argument. For example,

$$\Psi_{00} = 1 \tag{A.7a}$$

$$\Psi_{10} = z, \qquad \Psi_{11} = -\frac{(x+iy)}{2} \tag{A.7b, c}$$

$$\Psi_{20} = \frac{1}{2}z^2 - \frac{1}{4}(x^2+y^2), \qquad \Psi_{21} = \frac{1}{2}z(-x-iy), \qquad \Psi_{22} = \frac{(x+iy)^2}{8}. \tag{A.7d, e, f}$$

Expansions of arbitrary order, N, can be developed using Eq. (A.6). But this implies $O(N^3)$ operations since $O(N/2)$ multiplies are required for each of the $O(N^2)$ multipoles. To reduce the operation count to $O(N^2)$ one employs recursion relationships developed by considering the integral relation, Eq. (A.3), and integrating by parts:

$$\begin{aligned} \Psi_{nm} &= \frac{i^m}{2\pi n!} \int_0^{2\pi} W^n e^{imu}\, du \\ &= \frac{i^m}{2\pi i m n!} \left\{ [W^n e^{imu}]_0^{2\pi} - \int_0^{2\pi} n W^{n-1} (-q e^{iu} + p e^{-iu}) e^{imu}\, du \right\} \\ &= -\frac{1}{m}(q\Psi_{n-1,m+1} + p\Psi_{n-1,m-1}). \end{aligned} \tag{A.8}$$

Another relation can be developed by noting

$$\begin{aligned} \Psi_{nm} &= \frac{i^m}{2\pi n!} \int_0^{2\pi} (z + i\{q e^{iu} + p e^{-iu}\}) W^{n-1} e^{imu}\, du \\ &= \frac{1}{n}(z\Psi_{n-1,m} + q\Psi_{n-1,m+1} - p\Psi_{n-1,m-1}). \end{aligned} \tag{A.9}$$

Combining the last two relations yields

$$(n+m)\Psi_{nm} = z\Psi_{n-1,m} - 2p\Psi_{n-1,m-1}, \tag{A.10}$$

which is applicable for all $0 \le m \le n-1$. For $m=n$, simply use $\Psi_{nn} = (-p)^n/n!$; to start the recursion, use $\Psi_{00}=1$ and $\Psi_{10}=z$; and finally, for $m=0$, use $\Psi_{n,-1} = -\Psi^*_{n,1}$.

In the fast summation algorithm, multipole coefficients are first computed explicitly upon the finest level boxes. Coarser level coefficients are then obtained from finer level ones by recursive shifting of the coefficients from one box center to another. Such shifting rules are readily developed for the Coulombic case using Eq. (A.3). To evaluate the multipoles about the shifted point $(p', q', z') \leftarrow (p+a, q+b, z+c)$, consider

$$[\Psi_{nm}]_{\{p',q',z'\}} = \frac{i^m}{2\pi n!}\int_0^{2\pi} \{W + c + i(be^{iu} + ae^{-iu})\}^n e^{imu}\, du. \tag{A.11}$$

The term in brackets can be expanded into powers of a, b, and c using the binomial theorem which results in $O(N^3)$ terms, but which can be rearranged to a form involving only $O(N^2)$ terms so that for an N-order expansion ($O(N^2)$ multipoles) a total of $O(N^4)$ operations would be required. A better way is to apply the shifts along p, q and then z separately, resulting in

$$[\Psi_{nm}]_{\{p',q,z\}} = \sum_{k=0}^{[(m+n)/2]} \frac{(-a)^k}{k!}[\Psi_{n-k,m-k}]_{\{p,q,z\}} \tag{A.12a}$$

$$[\Psi_{nm}]_{\{p',q',z\}} = \sum_{k=0}^{[(n-m)/2]} \frac{b^k}{k!}[\Psi_{n-k,m+k}]_{\{p',q,z\}} \tag{A.12b}$$

$$[\Psi_{nm}]_{\{p',q',z'\}} = \sum_{k=0}^{n-m} \frac{c^k}{k!}[\Psi_{n-k,m}]_{\{p',q',z\}}, \tag{A.12c}$$

which now require only $O(n)$ operations per multipole per shift for a total of $O(N^3)$ operations. These expressions are much simpler than traditional shifting expressions for spherical harmonics. However, they are not optimal. A complete shift of all multipoles can in fact be accomplished in only $O(N^2)$ operations using the discrete fast Fourier transform [16], although the operations are algebraically more involved and require modification to maintain efficiency for low-order multipole expansions.

The preceding expressions now allow construction of multipoles for pure Coulombic as well as (see below) screened Coulombic potentials. Next, consider the evaluation of the multipole expansion at an observation point. This requires evaluation of the functions ψ_{nm} defined in Eq. (A.13), which are linearly related to the product Y_{nm}/r^{n+1} and hence to the combination Ψ_{nm}/r^{2n+1}. Hence, the recursive evaluation procedures available for Ψ_{nm} are readily applied to evaluation of Ψ_{nm} also. Expressions for the spatial gradients required in Taylor series expansions are obtained from the integral relation.

$$\psi_{nm} = \frac{n!}{2\pi i^m}\int_0^{2\pi} W^{-(n+1)} e^{imu}\, du \tag{A.13}$$

$$\frac{Y_{nm}}{r^{n+1}} = c_{nm}\psi_{nm}, \qquad c_{nm} = c_{n,-m} = \sqrt{\frac{2n+1}{4\pi(n-m)!(n+m)!}} = \frac{2n+1}{4\pi C_{nm}}. \quad \text{(A.14a, b)}$$

Comparing Eqs. (A.4) and Eqs. (A.14) reveals

$$\psi_{nm} = \frac{1}{r^{2n+1}}\frac{C_{nm}}{c_{nm}}\Psi_{nm} = \frac{(n-m)!(n+m)!}{r^{2n+1}}\Psi_{nm}. \quad \text{(A.15)}$$

From Eq. (A.13), the gradients

$$\begin{pmatrix}\partial/\partial p\\ \partial/\partial q\\ \partial/\partial z\end{pmatrix}\psi_{nm} = -\frac{n!(n+1)}{2\pi i^m}\int_0^{2\pi} W^{-(n+2)}\begin{pmatrix}ie^{-iu}\\ ie^{+iu}\\ 1\end{pmatrix}e^{imu}\,du = -\begin{pmatrix}\psi_{n+1,m-1}\\ -\psi_{n+1,m+1}\\ \psi_{n+1,m}\end{pmatrix}, \quad \text{(A.16)}$$

or using the definitions for p and q, Eq. (A.2):

$$\nabla\psi_{nm} = [A]\begin{Bmatrix}\psi_{n+1,m-1}\\ \psi_{n+1,m}\\ \psi_{n+1,m+1}\end{Bmatrix}, \qquad [A] = -\frac{1}{2}\begin{bmatrix}1 & 0 & -1\\ i & 0 & i\\ 0 & 2 & 0\end{bmatrix}. \quad \text{(A.17a, b)}$$

Hence, the gradient is simply a linear combination of $\psi_{n+1,m+j}$. Moreover, because the coefficients in $[A]$ are independent of R, higher order derivatives are easily obtained as linear combinations of lower order ones.

In Appendix B, another expression for the gradient is required which is derived as follows. Following the same procedure used to derive Eq. (A.17) one obtains

$$\nabla\Psi_{nm} = [B]\begin{Bmatrix}\Psi_{n-1,m-1}\\ \Psi_{n-1,m}\\ \Psi_{n-1,m+1}\end{Bmatrix}, \qquad [B] = -\frac{1}{2}\begin{bmatrix}1 & 0 & -1\\ i & 0 & i\\ 0 & -2 & 0\end{bmatrix}, \quad \text{(A.18a, b)}$$

which upon using identity, Eq. (A.15) yields

$$\nabla(\psi_{nm}) = \frac{1}{r^2}[B][N_{nm}]\begin{Bmatrix}\psi_{n-1,m-1}\\ \psi_{n-1,m}\\ \psi_{n-1,m+1}\end{Bmatrix} - (2n+1)\frac{\psi_{nm}}{r^2}R \quad \text{(A.19a)}$$

$$[N_{nm}] = \text{diag}\{(n+m)(n+m-1), (n+m)(n-m), (n-m)(n-m-1)\}. \quad \text{(A.19b)}$$

Recurrence relationships for ψ_{nm} can be derived in a similar manner as for Ψ_{nm}. Similarly, shifting rules for ψ_{nm} are developed by expanding the integral representation about a shifted center. Now, however, one obtains an infinite series. As before, multipoles about the shifted point $(p', q', z') \leftarrow (p+a, q+b, z+c)$ are obtained by performing three successive shifts

along each Cartesian direction. Thus, for example,

$$[\psi_{nm}]_{\{p',q,z\}} = \frac{n!}{2\pi i^m}\int_0^{2\pi}(W+iae^{-iu})^{-(n+1)}e^{imu}\,du$$
$$= \frac{n!}{2\pi i^m}\int_0^{2\pi}W^{-(n+1)}\sum_{k=0}^{\infty}(-1)^k\binom{n+k}{k}\left(\frac{iae^{-iu}}{W}\right)^k e^{imu}\,du$$
$$= \sum_{k=0}^{\infty}\frac{(-a)^k}{k!}[\psi_{n+k,m-k}]_{\{p,q,z\}}. \tag{A.20a}$$

Similarly,

$$[\psi_{nm}]_{\{p',q',z\}} = \sum_{k=0}^{\infty}\frac{b^k}{k!}[\psi_{n+k,m+k}]_{\{p',q,z\}} \tag{A.20b}$$

$$[\psi_{nm}]_{\{p',q',z'\}} = \sum_{k=0}^{\infty}\frac{(-c)^k}{k!}[\psi_{n+k,m}]_{\{p',q',z\}}. \tag{A.20c}$$

The downward pass of the fast summation process may be formulated either in terms of a succession of Taylor series extrapolations from coarser to finer level box centers or else as shifts in the expansion products. The former employs repeated application of the relation given in Eq. (A.17), which, assuming that all derivatives to order N are retained in the Taylor series expansion, requires $O(N^6)$ operations (this follows since there are N^4 terms in the Taylor series expansion of each of the $(N+1)(N+2)/2$ multipole coefficients); the latter applies a truncated version of relations given in Eq. (A.20), which entails $O(N^3)$ operations assuming the series are truncated at the Nth term. Clearly, the shifted expansion exhibits more favorable computational complexity for large-order expansion; unfortunately, it is not easily applied to the screened Coulombic potentials of interest here and at present regular Taylor series expansions are invoked.

APPENDIX B

Application to Screened Coulombic Kernels

Implementation of the SMBF-based multipole expansion requires manipulation of the products Q_{mk} defined in Eqs. (9). It is somewhat easier to proceed by first deriving the required relationships using the spherical (unmodified) Bessel functions. The corresponding expressions for the SMBFs can then be obtained by appropriate substitutions of imaginary arguments. Consider the product $Y_{nm}\zeta_n(r)$, where $\zeta_n(r)$ is any of the *real* spherical Bessel functions. To expedite computation, it is useful to establish recurrence relations for the gradients of these products (note that the products themselves are most efficiently procured by using the recurrence relations for Y_{nm} and ζ_n separately).

To derive such a relation, first define

$$p^{\lambda}_{nm} = \psi_{nm}r^{n+1}\zeta_n(\lambda r) \quad \Rightarrow \quad Y_{nm}\zeta_n(\lambda r) = c_{nm}\,p^{\lambda}_{nm}. \tag{B.1a, b}$$

Also, the following identities for spherical Bessel functions are required:

$$\frac{d}{dx}\left(x^{n+1}\zeta_n(x)\right) = x^{n+1}\zeta_{n-1}(x), \qquad \frac{2n+1}{x}\zeta_n = \zeta_{n-1} + \zeta_{n+1}. \tag{B.2a, b}$$

From these relations,

$$\begin{aligned}\nabla\left(p^{\lambda}_{nm}\right) &= r^{n+1}\zeta_n\nabla\psi_{nm} + \lambda\psi_{nm}r^{n+1}\zeta_{n-1}\frac{R}{r} \\ &= \lambda\frac{r^{n+2}}{2n+1}(\zeta_{n+1}+\zeta_{n-1})\nabla\psi_{nm} + \lambda\psi_{nm}r^{n+1}\zeta_{n-1}\frac{R}{r},\end{aligned} \tag{B.3}$$

Next, using identies given in Eqs. (A.17) to (A.19),

$$\begin{aligned}(\zeta_{n+1}+\zeta_{n-1})\nabla\psi_{nm} = \zeta_{n+1}[A]\begin{Bmatrix}\psi_{n+1,m-1}\\ \psi_{n+1,m}\\ \psi_{n+1,m+1}\end{Bmatrix} + \zeta_{n-1}\frac{1}{r^2}[B][N_{nm}]\begin{Bmatrix}\psi_{n-1,m-1}\\ \psi_{n-1,m}\\ \psi_{n-1,m+1}\end{Bmatrix} \\ -(2n+1)\zeta_{n-1}\frac{\psi_{nm}}{r^2}R,\end{aligned} \tag{B.4}$$

which when substituting back into Eq. (B.3) produces

$$\nabla\left(p^{\lambda}_{nm}\right) = \frac{\lambda}{2n+1}\left([A]\begin{Bmatrix}\psi_{n+1,m-1}\\ \psi_{n+1,m}\\ \psi_{n+1,m+1}\end{Bmatrix}r^{n+2}\zeta_{n+1} + [B][N_{nm}]\begin{Bmatrix}\psi_{n-1,m-1}\\ \psi_{n-1,m}\\ \psi_{n-1,m+1}\end{Bmatrix}r^{n}\zeta_{n-1}\right), \tag{B.5a}$$

or

$$\nabla\left(p^{\lambda}_{nm}\right) = \frac{\lambda}{2n+1}[A]\left(\begin{Bmatrix}p^{\lambda}_{n+1,m-1}\\ p^{\lambda}_{n+1,m}\\ p^{\lambda}_{n+1,m+1}\end{Bmatrix} + [N_{nm}]\begin{Bmatrix}p^{\lambda}_{n-1,m-1}\\ -p^{\lambda}_{n-1,m}\\ p^{\lambda}_{n-1,m+1}\end{Bmatrix}\right) \tag{B.5b}$$

(note the negative sign for $p^{\lambda}_{n-1,m}$). For $n = m = 0$, use

$$\nabla p^{\lambda}_{00} = \nabla\zeta_0 = -\frac{\lambda R}{r}\zeta_1 = -\lambda\zeta_1\frac{r^2}{2}\begin{bmatrix}1 & 0 & -1\\ i & 0 & i\\ 0 & 2 & 0\end{bmatrix}\begin{Bmatrix}\psi_{1,-1}\\ \psi_{1,0}\\ \psi_{1,1}\end{Bmatrix} = \lambda[A]\begin{Bmatrix}p^{\lambda}_{1,-1}\\ p^{\lambda}_{1,0}\\ p^{\lambda}_{1,1}\end{Bmatrix}, \tag{B.6}$$

which is the same as Eq. (B.5b) but dropping the last term. Fortunately, the coefficients and matrices are all independent of coordinates, thus greatly facilitating construction of higher order gradients. Equation (B.5b) agrees with Eq. (7.2.32) in Ref. [41] except for the derivative with respect to z, which reads

$$\frac{\partial}{\partial z}(\overline{Y}_{nm}\zeta_n) = \frac{\lambda}{2n+1}\{(n+m)\overline{Y}_{n-1,m}\zeta_{n-1} - (n-m+1)\overline{Y}_{n+1,m}\zeta_{n+1}\}, \tag{B.7}$$

To develop analogous expressions for the *modified* spherical Bessel functions, use

$$\hat{K}_{n+1/2}(z) \equiv \sqrt{\frac{\pi}{2z}} K_{n+1/2}(z) = -\frac{\pi}{2} i^n h_n^{(1)}(iz). \tag{B.8}$$

Hence, setting $\lambda = i\kappa$, substituting

$$\zeta_n(\lambda r) = h_n^{(1)}(i\kappa r) = -\frac{2}{\pi i^n} \hat{K}_{n+1/2}(\kappa r), \tag{B.9}$$

defining

$$q_{nm}^{\kappa} \equiv \psi_{nm} r^{n+1} \hat{K}_{n+1/2}(\kappa r) = -\frac{\pi}{2} i^n p_{nm}^{i\kappa}, \tag{B.10}$$

and inserting into Eq. (B.5), one obtains

$$\nabla\left(q_{nm}^{\kappa}\right) = \frac{\kappa}{2n+1}[A]\left(\begin{Bmatrix} q_{n+1,m-1}^{\kappa} \\ q_{n+1,m}^{\kappa} \\ q_{n+1,m+1}^{\kappa} \end{Bmatrix} - [N_{nm}] \begin{Bmatrix} q_{n-1,m-1}^{\kappa} \\ -q_{n-1,m}^{\kappa} \\ q_{n-1,m+1}^{\kappa} \end{Bmatrix}\right), \tag{B.11}$$

which is identical to Eq. (B.5) except for the reversed sign before $[N_{nm}]$. Again, the last term is discarded for the case,$n = m = 0$.

Finally, both p_{nm}^{λ} and q_{nm}^{κ} exhibit singular behavior when λ or $\kappa \to 0$, and it is preferable to operate with the products $(\lambda^{n+1} p_{nm}^{\lambda})$ and $(\kappa^{n+1} q_{nm}^{\kappa})$ respectively, which remain well behaved for all λ or κ provided $r > 0$. The latter product is related to the term $Q_{nm}(\kappa, R)$ defined in Eq. (9):

$$\kappa^{n+1} q_{nm}^{\kappa} = \frac{\pi \cdot 1 \cdot 3 \cdots (2n-1)\left(Q_{nm}^{\kappa}\right)^*}{2}. \tag{B.12}$$

Substituting into Eq. (B.11) shows

$$\nabla Q_{nm}^{\kappa} = [A^*]\left(\begin{Bmatrix} Q_{n+1,m-1}^{\kappa} \\ Q_{n+1,m}^{\kappa} \\ Q_{n+1,m+1}^{\kappa} \end{Bmatrix} - \frac{\kappa^2}{(2n-1)(2n+1)}[N_{nm}] \begin{Bmatrix} Q_{n-1,m-1}^{\kappa} \\ -Q_{n-1,m}^{\kappa} \\ Q_{n-1,m+1}^{\kappa} \end{Bmatrix}\right), \tag{B.13}$$

where $[A^*]$ is the matrix, $[A]$, with all elements replaced by their complex conjugates.

ACKNOWLEDGMENTS

The authors thank Magnus Ullner for providing us with coordinates of the linear polyelectrolyte chains. This work has been supported by the NIH under SBIR Phase II Grant GM50132.

REFERENCES

1. M. Abramowitz and I. A. Stegun, *Handbook of Mathematical Functions* (U.S. Department of Commerce, 1968).
2. T. M. A. O. M. Barenbrug, J. A. M. Smit, and D. Bedeaux, Conformational free energy of lattice polyelectrolytes with fixed endpoints. I. Single-chain simulation and theory, *Macromolecules* **30**, 605 (1997).
3. R. Bharadwaj, A. Windemuth, S. Sridharan, B. Honig, and A. Nicholls, The fast multipole boundary element method for molecular electrostatics: An optimal approach for large systems, *J. Comput. Chem.* **16**, 898 (1995).

4. T. C. Bishop, D. Kosztin, and K. Schulten, How hormone receptor–DNA binding affects nucleosomal DNA: The role of symmetry, *Biophys. J.* **72**, 2056 (1997).
5. T. C. Bishop, R. D. Skeel, and K. Schulten, Difficulties with multiple time stepping and fast multipole algorithm in molecular dynamics, *J. Comput. Chem.* **18**, 1785 (1997).
6. J. A. Board, Jr., J. W. Causey, J. F. Leathrum, Jr., A. Windemuth, and K. Shulten, Accelerated molecular dynamics simulation with the parallel fast multipole algorithm, *Chem. Phys. Lett.* **198**, 89 (1992).
7. C. Brender and M. Danino, Screening in short polyelectrolyte chains: A Monte Carlo study, *J. Phys. Chem.* **100**, 17563 (1996).
8. M. Challacombe, C. White, and M. Head-Gordon, Periodic boundary conditions and the fast multipole method, *J. Chem. Phys.* **107**, 10131 (1997).
9. T. E. Cheatham II, J. L. Miller, T. Fox, T. A. Darden, and P. A. Kollman, Molecular dynamics simulations on solvated biomolecular systems: The particle mesh Ewald method leads to stable trajectories of DNA, RNA, and proteins, *J. Am. Chem. Soc.* **117**, 4193 (1995).
10. H. Cheng, L. Greengard, and V. Rokhlin, *A Fast Adaptive Multipole Algorithm in Three Dimensions*, Research Report YALEU/DCS/RR-1158, Department of Computer Science, Yale University (1998).
11. G. A. Christos and S. L. Carnie, Computer simulations of polyelectrolyte chains in salt solution, *J. Chem. Phys.* **92**, 7661 (1990).
12. T. Darden, D. York, and L. Pedersen, Particle mesh Ewald: An Nlog(N) method for Ewald sums in large systems, *J. Chem. Phys.* **98**, 10089 (1993).
13. J. J. Delrow, J. A. Gebe, and J. M. Schurr, Comparison of hard-cylinder and screened coulomb interactions in the modeling of supercoiled DNAs, *Biopolymers* **42**, 455 (1997).
14. M. Deserno and C. Holm, How to mesh up Ewald sum. I. A theoretical and numerical comparison of various particle–mesh routines, *J. Chem. Phys.* **109**, 7678 (1998).
15. H.-Q. Ding, N. Karasawa, and W. A. Goddard III, Atomic level simulations on a million particles: The cell multipole method for Coulomb and London nonbond interactions, *J. Chem. Phys.* **97**, 4309 (1992).
16. W. D. Elliott and J. A. Board, Jr., *Fast Fourier Transform Accelerated Fast Multipole Algorithm*, Technical Report 94-001, Duke University (1994).
17. M. A. Epton and B. Dembart, Multipole translation theory for the three-dimensional Laplace and Helmholtz equations, *SIAM J. Sci. Comput.* **16**, 865 (1995).
18. U. Essmann, L. Perera, M. L. Berkowitz, T. Darden, H. Lee, and L. G. Pedersen, A smooth particle mesh Ewald method, *J. Chem. Phys.* **103**, 8577 (1995).
19. R. T. Farouki and S. Hamaguchi, Thermodynamics of strongly-coupled Yukawa systems near the one-component-plasma limit. II. Molecular dynamics simulations, *J. Chem. Phys.* **101**, 9885 (1994).
20. M. O. Fenley, W. K. Olson, K. Chua, and A. H. Boschitsch, Fast adaptive multipole method for computation of electrostatic energy in simulations of polylectrolyte DNA, *J. Comput. Chem.* **17**, 976 (1996).
21. M. O. Fenley, W. K. Olson, I. Tobias, and G. S. Manning, Electrostatic effects in short superhelical DNA, *Biophys. Chem.* **50**, 255 (1994).
22. F. Figueirido, R. M. Levy, R. Zhou, and B. J. Berne, Large scale simulation of macromolecules in solution: Combining the periodic fast multipole method with multiple time step integrators, *J. Chem. Phys.* **106**, 9835 (1997).
23. L. Greengard and V. Rokhlin, A fast algorithm for particle simulations, *J. Comput. Phys.* **73**, 325 (1987).
24. L. Greengard and V. Rokhlin, On the evaluation of electrostatic interactions in molecular modeling, *Chem. Scripta* **29A**, 139 (1989).
25. L. Greengard and V. Rokhlin, A new version of the fast multipole method for the Laplace equation in three dimensions, *Acta Numer.* **229** (1997).
26. L. F. Greengard, *The Rapid Evaluation of Potential Fields in Particle Systems* (MIT Press, Cambridge, MA, 1988).
27. L. F. Greengard and V. Rokhlin, *Rapid Evaluation of Potential Fields in Three-Dimensions*, Technical Report 515, Computer Science Department, Yale University (1987).
28. S. Hamaguchi, R. T. Farouki, and D. H. E. Dubin, Phase diagram of Yukawa systems near one-component-plasma limit revisited, *J. Chem. Phys.* **105**, 7641 (1996).

29. H. H. Hooper, S. Beltran, A. P. Sassi, H. W. Blanch, and J. M. Prausnitz, Monte Carlo simulations of hydrophobic polyelectrolytes: Evidence for a structural transition in response to increasing chain ionization, *J. Chem. Phys.* **93**, 2715 (1990).
30. T. Hrycak and V. Rokhlin, An improved fast multipole algorithm for potential fields, *SIAM J. Sci. Comput.* **19**, 1804 (1998).
31. G. T. Ibragimova and R. C. Wade, Importance of explicit salt ions for protein stability in molecular dynamics simulation, *Biophys. J.* **74**, 2906 (1998).
32. A. H. Juffer, E. F. F. Botta, B. A. M. v. Keulen, A. v. d. Ploeg, and H. J. C. Berendsen, The electric potential of a macromolecule in a solvent: A fundamental approach, *J. Comput. Phys.* **97**, 144 (1991).
33. K. Kremer, M. O. Robbins, and G. S. Grest, Phase diagram of Yukawa systems: Model for charge-stabilized colloids, *Phys. Rev. Lett.* **57**, 2694 (1986).
34. J. Liang and S. Subramaniam, Computation of molecular electrostatics with boundary elements methods, *Biophys. J.* **73**, 1830 (1997).
35. K.-T. Lim, S. Brunett, M. Iotov, R. B. McClurg, N. Vaidhi, S. Dasgupta, S. Taylor, and W. A. Goddard III, Molecular dynamics for very large systems on massively parallel computers: The MPSim program, *J. Comput. Chem.* **18**, 501 (1997).
36. S. R. Lustig, J. J. Cristy, and D. A. Pensak, The fast multipole method in canonical ensemble dynamics on massively parallel computers, *Mat. Res. Soc. Symp. Proc.* **278**, 9 (1992).
37. B. A. Luty, M. E. Davis, I. G. Tironi, and W. F. van Gunsteren, A comparison of particle–particle, particle–mesh, and Ewald methods for calculating electrostatic interactions in periodic molecular systems, *Mol. Simul.* **14**, 11 (1994).
38. B. A. Luty and W. F. van Gunsteren, Calculating electrostatic interactions using the particle–particle–particle–mesh method with nonperiodic long-range interactions, *J. Phys. Chem.* **100**, 2581 (1996).
39. A. M. Mathiowetz, A. Jain, N. Karasawa, and W. A. Goddard III, Protein simulations using techniques suitable for very large systems: The cell multipole method for nonbond interactions and the Newton–Euler inverse mass operator method for internal coordinate dynamics, *Proteins Struct. Funct, Genet.* **20**, 227 (1994).
40. H. Merlitz, K. Rippe, K. V. Klenin, and J. Langowski, Looping dynamics of linear DNA molecules and the effect of DNA curvature: A study by Brownian dynamics simulation, *Biophys. J.* **74**, 773 (1998).
41. P. M. Morse and K. U. Ingard, *Theoretical Acoustics* (McGraw–Hill, New York, 1968).
42. H. G. Peterson, D. Soelvason, J. W. Perram, and E. R. Smit, The very fast multipole method, *J. Chem. Phys.* **101**, 8870 (1994).
43. E. L. Pollock and J. Glosli, Comments on P3M, FMM, and the Ewald method for large periodic Coulombic systems, *Comput. Phys. Commun.* **95**, 93 (1996).
44. E. O. Purisima, Fast summation boundary element method for calculating solvation free energies of macromolecules, *J. Comput. Chem.* **19**, 1494 (1998).
45. J. Rahola, *Diagonal Forms of the Translation Operators in the Fast Multipole Algorithms for Scattering Problems*, Research Report, Helsinki University of Technology, Institute of Mathematics (1995).
46. C. E. Reed and W. F. Reed, Monte Carlo study of light scattering by linear polyelectrolytes, *J. Chem. Phys.* **97**, 7766 (1992).
47. V. Rokhlin, Diagonal forms of translation operators for the Helmholtz equation in three dimensions, *Appl. Comput. Harmon. Anal.* **1**, 82 (1993).
48. W. B. Russel, D. A. Saville, and W. R. Schowalter, *Colloidal Dispersions* (Cambridge Univ. Press, Cambridge, UK, 1991).
49. J. K. Salmon, *Parallel Hierarchical N-Body Methods*, Ph.D. thesis, California Institute of Technology (1991).
50. H. Samet, *The Design and Analysis of Spatial Structures* (Addison–Wesley, Reading, MA, 1990).
51. T. Schlick, B. Li, and W. K. Olson, The influence of salt on the structure and energetics of supercoiled DNA, *Biophys. J.* **67**, 2146 (1994).
52. T. Schlick and W. K. Olson, Trefoil knotting revealed by molecular dynamics simulations of supercoiled DNA, *Science* **257**, 1110 (1992).
53. K. E. Schmidt and M. A. Lee, Implementing the fast multipole method in three dimensions, *J. Stat. Phys.* **63**, 1223 (1991).

54. R. Sedgewick, *Algorithms* (2nd, Addison–Wesley, Reading, MA, 1988).
55. J. Shimada, H. Kaneko, and T. Takada, Performance of fast multipole methods for calculating electrostatic interactions in biomacromolecular simulations, *J. Comput. Chem.* **15**, 28 (1994).
56. O. N. de Souza and R. L. Ornstein, Inherent DNA curvature and flexibility correlate with TATA box functionality, *Biopolymers* **46**, 403 (1998).
57. B. Svensson and B. Jönsson, On the mean spherical approximation (MSA) for colloidal systems. A comparison with results from Monte Carlo simulations, *Mol. Phys.* **50**, 489 (1983).
58. M. C. Tesi, E. J. Janse van Rensburg, E. Orlandini, D. W. Sumners, and G. S. Whittington, Knotting and supercoiling in circular DNA: A model incorporating the effect of added salt, *Phys. Rev. E* **49**, 868 (1994).
59. H. Totsuji, T. Kishimoto, and C. Totsuji, Structure of confined Yukawa system (dusty plasma), *Phys. Rev. Lett.* **78**, 3113 (1997).
60. A. Y. Toukmaji and J. A. J. Board, Ewald summation techniques in perspective: A survey, *Comput. Phys. Commun.* **95**, 73 (1996).
61. M. Ullner and B. Jönsson, A Monte Carlo study of titrating polyelectrolytes, *J. Chem. Phys.* **104**, 3048 (1996).
62. M. Ullner, B. Jönsson, C. Peterson, O. Sommelius, and B. Söderberg, The electrostatic persistence length calculated from Monte Carlo, variational and pertubation methods, *J. Chem. Phys.* **107**, 1279 (1997).
63. V. Vlachy, C. Pohar, and A. D. J. Haymet, Structure and thermodynamics of the screened Coulomb liquid, *J. Chem. Phys.* **88**, 2066 (1988).
64. A. Vologodskii and N. Cozzarelli, Modeling of long-range electrostatic interactions in DNA, *Biopolymers* **35**, 289 (1995).
65. P. Welch and M. Muthukumar, Tuning the density profile of dendritic polyelectrolytes, *Macromolecules* **31**, 5892 (1998).
66. C. A. White and M. Head-Gordon, Derivation and efficient implementation of the fast multipole method, *J. Chem. Phys.* **101**, 6593 (1994).
67. M. Wojcik, Computer simulation of ion migration in ionic micellar systems, *Chem. Phys. Lett.* **260**, 287 (1996).
68. B. J. Yoon and A. M. Lenhoff, A boundary element method for molecular electrostatics with electrolyte effects, *J. Comput. Chem.* **11**, 1080 (1990).
69. M. A. Young and D. L. Beveridge, Molecular dynamics simulations of oligonucleotide duplex with adenine tracts phased by a full helix turn, *J. Mol. Biol.* **281**, 675 (1998).
70. R. J. Zauhar and A. Varnek, A fast and space efficient boundary element method for computing electrostatic and hydration effects in large molecules, *J. Comput. Chem.* **17**, 864 (1996).